Intra-urban nocturnal cooling rates: model development and evaluation

S. Onomura[1], B. Holmer[1], F. Lindberg[1], S. Thorsson[1]
[1] *Department of Earth Sciences, University of Gothenburg, Box 460, Gothenburg SE-405 30, Sweden*
shiho.onomura@gu.se

dated : 15 June 2015

1. Introduction

The urban heat island (UHI) and the intra-urban heat island (IUHI) are mainly nocturnal phenomena that develop through differences in cooling between urban and rural sites or between intra-urban sites of various types (Eliasson 1994; Runnalls and Oke 2000). These differences are a result of site characteristics such as building density, surface material, amount of vegetation and presence of anthropogenic heat (Oke 1987). It has been observed that nocturnal cooling progresses in two distinct phases (phase 1: site-dependent cooling around sunset, and phase 2: site-independent cooling from about one or two hours after sunset until sunrise) (Oke and Maxwell 1975; Upmanis et al. 1998; Holmer et al. 2007; Holmer et al. 2013). In this study, the temporal development of nocturnal cooling was investigated especially focusing on the two phases using observational data from Gothenburg, Sweden (Onomura et al. 2015). Based on the data analysis, a NOcturnal Cooling RAte Model (NOCRAM) was analytically developed to simulate nocturnal air temperature at urban sites using standard meteorological variables and sky view factor of the site. The model is evaluated with other datasets in the city and further applied to one built-up site with complex urban geometry in London UK.

2. Model development

2.1 Model structure

A conceptual profile of nocturnal cooling rates typical for open sites under ideal (clear and calm) conditions is shown in figure 1. The temporal development of cooling rates is partitioned into three parts, phase 1A, 1B and 2, which are drawn by red, blue and green thick lines. As a basic profile, the cooling rate curve is firstly created in the model. Initial cooling rate (CR_1) of phase 1A is calculated using observed air temperature. Phase 1A and 1B are modelled with cosine functions using CR_1, most intensive cooling rate (CR_{peak}) in phase 1 and initial cooling rate (CR_2) of phase 2. The angles applied to the two phases range from 0 to π and π to 2π, respectively. Phase 2 is modelled with a linear function using CR_2 under the assumption that cooling ends at sunrise. The profile is modified every time step by estimating the impact of the temporal changes in wind speed ($\Delta CR_w(t)$) on cooling rates (grey thin line in Figure 1). Cooling rates (CR) in the three phases are calculated as follows:

$$\text{Phase 1A: } CR = (CR_1 - CR_{peak})\cdot(\cos(f(t-t_1))-1)/2 + CR_1 + \Delta CR_w(t) \quad \text{when } t_1 \le t < t_{peak} \quad (1)$$

$$\text{Phase 1B: } CR = (CR_2 - CR_{peak})\cdot(\cos(f(t-t_{peak}))-1)/2 + CR_{peak} + \Delta CR_w(t) \quad \text{when } t_{peak} \le t < t_2 \quad (2)$$

$$\text{Phase 2: } CR = (t_{end}-t)/(t_{end}-t_2)\cdot CR_2 + \Delta CR_w(t) \quad \text{when } t_2 \le t < t_{end} \quad (3)$$

where function f converts time into radian, t_1 and t_2 are the onset of phase 1A and 2, t_{peak} is the timing of the most intensive cooling and t_{end} is the end of phase 2. CR_{peak}, CR_2 and $\Delta CR_w(t)$ as well as t_1, t_2, t_{peak} and t_{end} have to be determined to simulate a nocturnal cooling rate profile. The procedure for determining these variables is based on the data analysis in Onomura et al. (2015) and summarized in 2.2 – 2.5. Note that the current version of the model does not take into account the impacts of anthropogenic heat, latent heat (e.g. from vegetation and precipitation) and synoptic weather changes (e.g. cold fronts) on cooling rates.

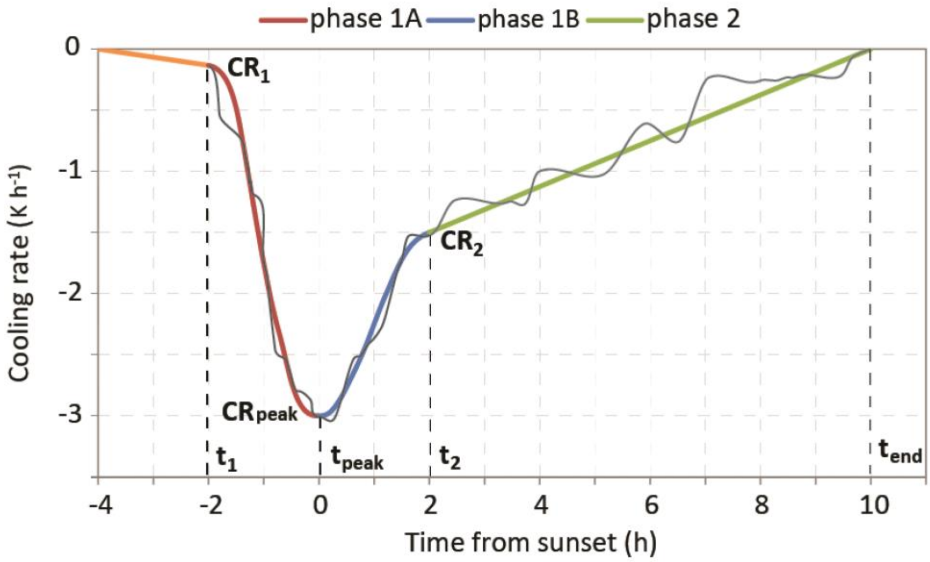

Fig. 1 A conceptual profile of cooling rates for open sites under ideal (clear and calm) conditions. The start and end of the three phases are indicated by t_1, t_{peak}, t_2 and t_{end}. Initial cooling rate of phase 1A (CR_1), most intensive cooling rate (CR_{peak}) and initial cooling rate of phase 2 (CR_2) are shown. A grey line around the profile illustrates how weather changes such as wind and cloud cover/type affect cooling rates during the night.

2.2 Time-related parameters

The onset of phase 1A and 2 was found to depend on the decay of daytime turbulence. As a measure of the strength of turbulence, relative wind speed change (the ratio of wind speed change per hour to hourly average wind speed) was introduced. t_1 is defined as the time between three and a half hours before sunset to sunset when relative wind speed change falls below -0.2 s^{-1}, and is negative in the previous time step. Similarly, t_2 is determined as one hour after the time between one hour before sunset to four hours after sunset when relative wind speed change falls below -0.5 s^{-1}. If t_2 is earlier than t_1, t_2 is set to be the next time step of t_1. Default values taken from figure 7 in Onomura et al. (2015) are prepared for the case when t_1 and t_2 cannot be determined because relative wind speed change does not meet the conditions. t_{peak} is simply calculated as the middle time between t_1 and t_2. t_{end} is set to sunrise.

2.3 Determination of most intensive cooling rate (CR_{peak}) in phase1

CR_{peak} is estimated by first considering the impact of clearness index of the sky (*CI*), average wind speed ±3 h around sunset (*U*) and maximum daily air temperature (T_{max}), and followed by the impact of *SVF*. *CI* is calculated as the ratio of the measured solar irradiance to the clear-sky irradiance based on the Crawford and Duchon (1999) method, modified by Lindberg et al. (2008), and averaged between noon and sunset for three hours after the sunrise on the next day. The magnitude of CR_{peak} was found to increase with higher *CI* and decreases with *U*. The influence of *CI* and *U* is handled by the introduction of the Cooling Rate Impact Factor (*CRIF*). As shown in figure 2a, this index takes the value of 1 under clear sky (*CI* = 1, named CI_{max}) and calm (*U* = 0) condition and decreases as *CI* decreases and *U* increases. *CRIF* is 0 when *CI* is below a critical value (CI_{min} set to 0.4) and/or *U* exceeds a threshold value (U_{crit} set to 4 m s^{-1}). Thereby, *CRIF* is expressed as:

$$CRIF = (1 - U/U_{crit})\cdot(CI - CI_{min})/(CI_{max} - CI_{min}) \qquad (4)$$

Further, the magnitude of CR_{peak} was observed to increase with higher T_{max} under a certain condition of *CI* and *U*, thus given *CRIF*. The linear fit for clear and calm condition was derived from the data analysis in Onomura et al. (2015) and assigned *CRIF* = 0.72 calculated using the average values of *CI* and *U* (Fig. 2b). Two assumptions were then introduced. Firstly, the slope and intercept of the linear relationship between CR_{peak} and T_{max} scales with *CRIF*. Secondly, at *CRIF* = 0 (overcast and windy condition) CR_{peak} does not change with T_{max} and is equal to the minimum value of CR_{peak} set to - 0.2 K h^{-1}. Thus, CR_{peak} can be expressed as a function of T_{max} and *CRIF*:

$$CR_{peak} = -0.2 + a\cdot(T_{max} + 13) \qquad (5)$$

$$a = -0.083\cdot CRIF \quad (6)$$

The relationship is shown in figure 2b for *CRIF* from 0 to 1.

The influence of *SVF* on CR_{peak} is handled by introducing the Sky View Impact Factor (*SVIF*), which is the ratio of CR_{peak} at a built-up site to an open site. The value of *SVIF* decreases with higher *SVF* under a certain condition of *CI* and *U*. In the same way as figure 2b, the trend line for clear and calm condition was derived from the data analysis and assigned the average *CRIF* = 0.72. Under cloudy condition (average *CRIF* = 0.20) *SVF* was found to have little impact on CR_{peak}, so *SVIF* was set to 0.99, which was treated as a threshold value below which *SVIF* does not change with *SVF*. Assuming that the relationship between *SVIF* and *SVF* scales linearly with *CRIF*, *SVIF* can be then expressed as:

$$SVIF = CR_{peak,\ built\text{-}up}/CR_{peak,\ open} = 0.99 + b \cdot (1 - SVF) \quad (7)$$

$$b = -0.88 \cdot (CRIF - 0.2)/(1 - 0.2) \quad (8)$$

which is shown graphically in figure 2c.
Using *SVIF*, CR_{peak} is finally expressed as:

$$CR_{peak} = [-0.2 - 0.083 \cdot CRIF \cdot (T_{max} + 13)] \cdot SVIF \quad (9)$$

2.4 Determination of initial cooling rate in phase 2 (CR_2)

The magnitude of CR_2 was found to increase with lower hourly average wind speed at t_2 (U_2) under a certain condition of *CI*. The line trend under clear condition is derived from the data analysis and assigned the average *CI* = 0.96. It was also found that under cloudy condition (average *CI* = 0.57) CR_2 changes little with U_2. The line of *CI* = 0.57 is used to determine the minimum magnitude of CR_2. Assuming that the relationship between CR_2 and U_2 scales linearly with *CI* and that when $U_2 \geq 2$ m s^{-1}, CR_2 follows the line of *CI* = 0.57, CR_2 is expressed as:

$$CR_2 = CR_{2\_min} + (CR_{2\_clear} - CR_{2\_min}) \cdot (CI - 0.57) / (1 - 0.57) \quad (10)$$

$$CR_{2\_clear} = -1.6 + 0.67 \cdot U_2 \quad (11)$$

$$CR_{2\_min} = -0.34 + 0.03 \cdot U_2 \quad (12)$$

The relationship is shown in figure 2d for *CI* from 0.57 to 1.

2.5 Modelling the impact of wind change

Cooling rates are affected by changes in weather, particularly wind and cloudiness. The effects of wind speed changes are considered in the model but cloudiness changes are not since cloud data are often not available during night. Every time step, the wind impact is estimated as a function of the third root of the difference between wind speed at the time step and average wind speed of the phase ($\bar{U}_{phase1A}$, $\bar{U}_{phase1B}$ and $\bar{U}_{phase2}$). The use of the third root was determined by the sensitivity test, which showed that the impact of small wind speed changes on cooling rates is reasonably estimated using the third root rather than other formulas. The transition of atmospheric stability from unstable to stable is found to occur around t_{peak}. It is suggested that higher wind speed brings colder air from above the canopy layer and enhances cooling rates in phase 1A, whereas it brings warmer air from above and diminishes cooling rates in phase 1B and 2. In addition, weak wind promotes mixing the air down to the ground (Acevedo and Fitzjarrald 2003). Therefore, higher wind speed than the average wind speed increases the magnitude of cooling rates during phase 1A, whereas it decreases during phase 1B and 2. The case of lower wind speed than the average wind speed is the other way around. Furthermore, the magnitude of the wind impact on cooling rates should decrease under cloudier condition due to weaker stratification of the atmosphere. Therefore, the Wind Impact Factor (WIF) is introduced to adjust the impact depending on *CI*. *WIF* is set to 0.35, 0.15 and 0.1 under clear (CI ≥ 0.9), semi-cloudy (0.75 ≤ CI < 0.9) and cloudy (CI < 0.75) conditions, respectively. Finally, the variation of cooling rate caused by the wind speed change at time *t* ($\Delta CR_w(t)$) is estimated as

$$\Delta CR_w(t) = \begin{cases} -WIF \cdot (U(t) - \bar{U}_{phaseX})^{1/3}, & \text{if } X = 1A \\ +WIF \cdot (U(t) - \bar{U}_{phaseX})^{1/3}, & \text{if } X = 1B \text{ or } 2 \end{cases} \quad (13)$$

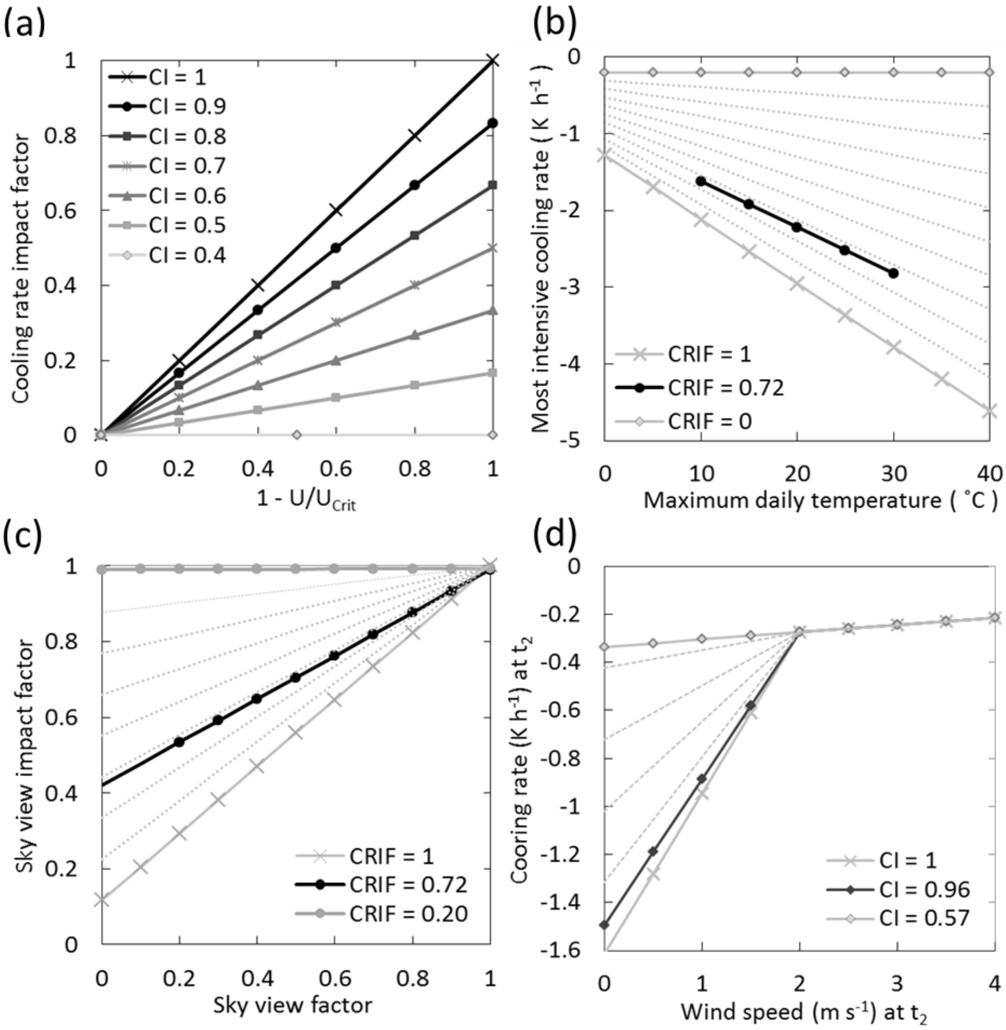

Fig. 2 Determination of most intensive cooling rates (CR_{peak}) using (a) average wind speed around sunset (U) and critical wind speed (U_{crit} set to 4 m s^{-1}), (b) maximum daily air temperature (T_{max}) and (c) sky view factor (SVF), and (d) determination of initial cooling rates (CR_2) in relation to hourly averaged wind speed at the start of phase 2 (t_2).

3. Model evaluation

3.1 Study site and data

An open site (*SVF* = 0.92) and a built-up site (*SVF* = 0.40) in Gothenburg Sweden and one built-up site (*SVF* = 0.46) in London UK were chosen for model evaluation. The former two sites are located in the city centre with most buildings having three to six stories and being almost regularly arranged. The site in London is located at the Barbican Estate, which has very complex urban settings and a large variation in building height. The sites mentioned were not used for the model parameterisation. Meteorological input data are taken from nearby reference meteorological stations (LUMA ; Onomura et al. 2015). The *SVF* representing each site was taken to be the average *SVF* within a 25 m radius, calculated using digital surface models of buildings and vegetation as described in Lindberg and Grimmond (2010) and using the ArcMap 10.1 software.

3.2 Model performance

The mean profiles of modelled and observed cooling rates and air temperature for the three sites for the three *CI* classes are shown in figure 3. The model simulates cooling rates well for all the sites. From the profiles of the open site (first column), it is clearly seen that the model successfully estimates the magnitude of cooling rates decreasing with lower *CI*. Also the two phases in cooling are modelled as less distinct under cloudier condition. In comparison with a built-up site in Gothenburg (second column), the model is successful to reduce the magnitude of cooling rates in phase 1 with lower *SVF* under all the cloud conditions. For the built-up site in London, cooling rates are modelled with the performance as good as Gothenburg. This suggests that the model is able to simulate cooling rates at built-up sites with complex urban geometry using only *SVF*. For CI ≥ 0.9, standard deviations are large. This is due to a small number of the samplings, but also because of the large variation of wind speed probably related to the complex geometry. Using the modelled cooling rates, nocturnal air temperature is estimated with high accuracy ($R^2 \geq 0.80$ and RMSE ≤ 1.61).

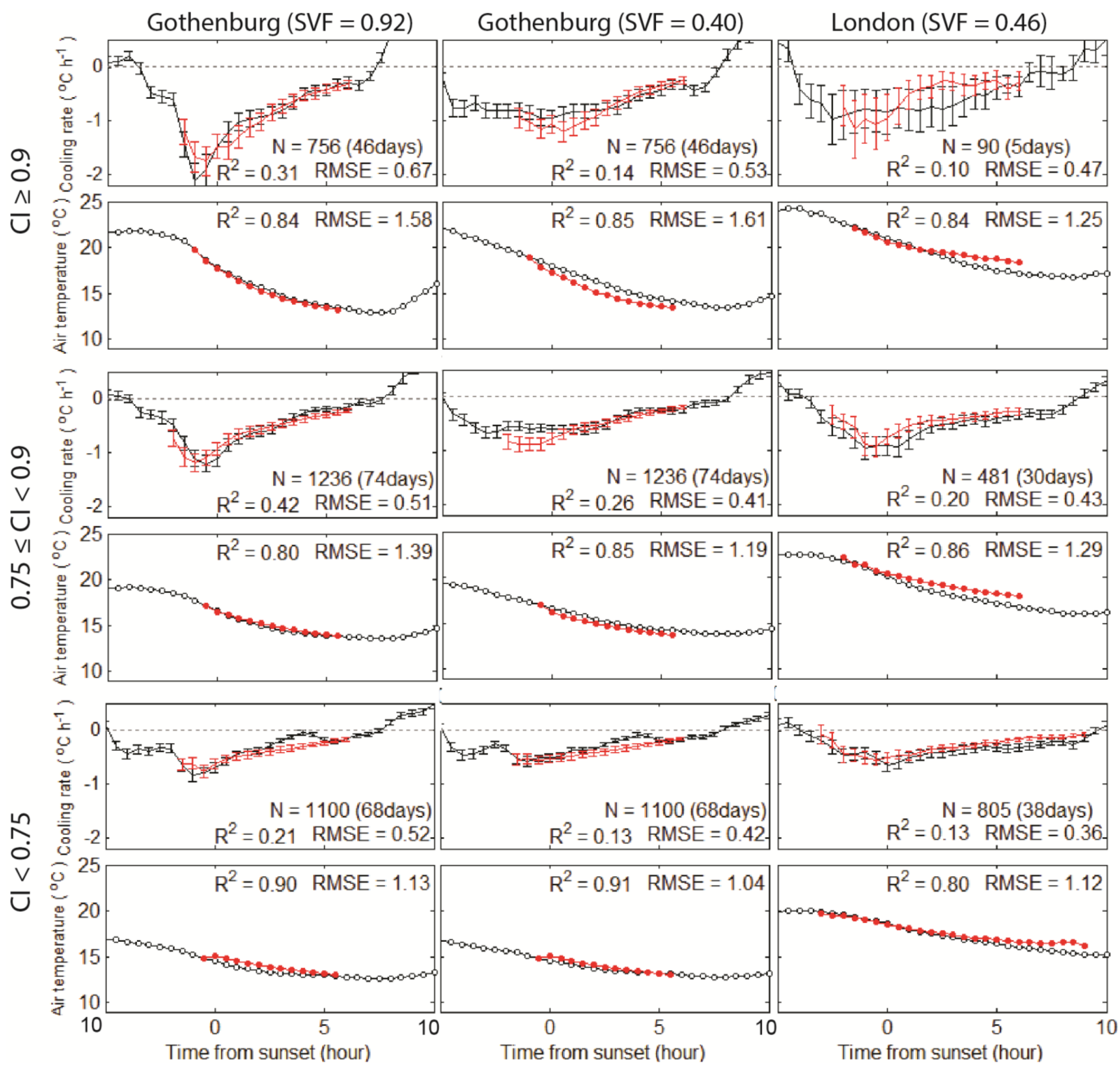

Fig. 3 Average profiles of modelled (red) and observed (black) cooling rate and air temperature for an open site and a built-up site in Gothenburg and a built-up site in London for three classes of cloudiness (clear (CI ≥ 0.9), semi-cloudy (0.75 ≤ CI < 0.9) and cloudy (CI < 0.75) from top to bottom). Due to the different length of night, the modelled profile is shown when the number of samplings at the time is larger than half of the observational samplings. Vertical bars on the cooling rate profiles indicate the standard deviations. The coefficient of determination (R^2) and root mean square error (RMSE) are calculated for N data on the number of days shown in the parenthesis.

5. Conclusion

The NOcturnal Cooling RAte Model (NOCRAM) was analytically developed specifically to represent the process of nocturnal cooling progressing in two distinct phases, as well as to represent the relationships between cooling rates and sky-clearness, wind speed, maximum daily air temperature and sky view factor. The model requires commonly-used meteorological variables (i.e. incoming shortwave radiation, air temperature, relative air humidity, wind speed, and air pressure) as well as the geometric information (i.e. the sky view factor of the site and the geographical coordinates of reference meteorological station). The model simulates cooling rates well, capturing the characteristic development of cooling in the two phases under a wide range of wind and cloud conditions, as well as the effect of sky view factor on cooling rates. Using the modelled cooling rates, the temporal development of nocturnal air temperature is calculated with high accuracy. Due to its simplicity, the model can be easily used in climate applications, such as nocturnal human thermal comfort estimation and climate-sensitive urban planning and design.

Acknowledgment

This project is financially supported by the Swedish Research Council Formas, the Swedish Energy Agency, the Swedish Environmental Protection Agency, the Swedish National Heritage Board and the Swedish Transport Administration (214-2010-1706 and 250-2010-358). We appreciate Ms. Janina Konarska for operating the intra-urban air temperature measurement in Gothenburg during 2012 – 2014, and Mr. William Morrison and Dr. Simone Kotthaus for providing observational data from London.

References

Crawford, T. M., and C. E. Duchon, 1999: An improved parameterization for estimating effective atmospheric emissivity for use in calculating daytime downwelling longwave radiation. *Journal of Applied Meteorology*, **38,** 474-480.

Eliasson, I., 1994: Urban-suburban-rural air temperature differences related to street geometry. *Physical Geography*, **15,** 1-22.

Holmer, B., S. Thorsson, and I. Eliasson, 2007: Cooling rates, sky view factors and the development of intra-urban air temperature differences. *Geografiska Annaler Series a-Physical Geography*, **89A,** 237-248.

Holmer, B., S. Thorsson, and J. Lindén, 2013: Evening evapotranspirative cooling in relation to vegetation and urban geometry in the city of Ouagadougou, Burkina Faso. *International Journal of Climatology*, **33,** 3089-3105.

Lindberg, F., and C. S. B. Grimmond, 2010: Continuous sky view factor maps from high resolution urban digital elevation models. *Climate Research*, **42,** 177-183.

Lindberg, F., B. Holmer, and S. Thorsson, 2008: SOLWEIG 1.0 - Modelling spatial variations of 3D radiant fluxes and mean radiant temperature in complex urban settings. *International Journal of Biometeorology*, **52,** 697-713.

LUMA. *BFCL and BCT.* [Available online at http://www.met.reading.ac.uk/micromet/LUMA/LUMA.html.]**,** Accessed 2015-12-04.

Oke, T. R., 1987: *Boundary layer climates*. 2nd ed. Routledge, London and New York, 294 pp.

Oke, T. R., and G. B. Maxwell, 1975: Urban heat island dynamics in Montreal and Vancouver. *Atmospheric Environment*, **9,** 191-200.

Onomura, S., B. Holmer, F. Lindberg, and S. Thorsson, 2015: Urban nocturnal cooling rates: development and evaluation of the NOCRA Model. In Review *Theoretical and Applied Climatology.*

Runnalls, K. E., and T. R. Oke, 2000: Dynamics and controls of the near-surface heat island of Vancouver, British Columbia. *Physical Geography*, **21,** 283-304.

Upmanis, H., I. Eliasson, and S. Lindqvist, 1998: The influence of green areas on nocturnal temperatures in a high latitude city (Göteborg, Sweden). *International Journal of Climatology*, **18,** 681-700.